Applied Physics B
Lasers and Optics

CrossMark

Analytical model for transverse mode conversion at all-optically induced, transient long-period gratings: from continuous-wave to ultrafast

Tim Hellwig[1] · Kai Sparenberg[1] · Carsten Fallnich[1]

Abstract Transverse mode conversion at an index grating, all-optically induced by multi-mode interference and the optical Kerr effect, is commonly studied by numerical simulations relying on either multi-mode implementations of the generalized nonlinear Schrödinger equation or beam propagation methods. Here, we present and discuss an analytical model describing the directed energy exchange between two probe modes moderated by two control modes. The analytical model can be derived in a four-wave mixing representation as well as in a material representation in analogy to the different numerical approaches demonstrating their equivalence. The analytical nature of the model is used to provide general insight into the conversion process in dependence on phase mismatch as well as induced coupling strength. While being a continuous-wave model, the applicability of the model for mode conversion using ultrashort pulses is discussed and guidelines for using the model as a first estimate for experiments or for more precise but time-consuming numerical simulations are given.

1 Introduction

The control over the transverse modal content of optical fibers by means of periodic perturbation of light propagation has found many applications since the first introduction of permanent long-period gratings (LPGs) written point by point, using UV laser sources illuminating a photosensitive fiber from the side [1]. Applications of LPGs include tunable band-rejection filters [2–4], gain equalizers [5] and dispersion compensation [6–8] in the field of telecommunications. All of the above-mentioned long-period gratings have in common that they are permanently inscribed into the fiber.

Parallel to the development and application of fixed LPGs, a dynamic control of the modal content was found of interest and firstly realized by inducing flexural acoustic waves in a fiber [9–11]. While offering some flexibility, the rate by which these gratings can be changed is fundamentally limited by the speed of acoustic waves in glass, and acoustic gratings have not found a wide application yet. However, in general a fast and dynamic control of the modal content at a position of choice could be of high interest, e.g., in the context of ultrafast transverse switching for upcoming spatial division multiplexing systems [12]. In order to further scale data capacities, transverse eigenmodes of few-mode fibers are proposed to be used as a multiplicator for existing data channels in telecommunications [13, 14]. In this context, acousto-optical switching of transverse modes has very recently gained new interest [15]. However, as these switches are limited in the achievable switching speed to the order of tens of microseconds, one challenging aspect of using transverse modes for data communications remains the ultrafast routing and switching.

An ultrafast, flexible and noninvasive method for changing the transverse modal content of a fiber seemed not feasible using long-period gratings until Park et al. and others demonstrated an optically induced long-period grating (OLPG) making use of the dependence of the refractive index on the local intensity (the optical Kerr effect) as well as a multi-mode interference beating between two

✉ Tim Hellwig
  tim.hellwig@uni-muenster.de

[1] Optical Technologies, Institute of Applied Physics,
  Westfälische Wilhelms-Universität, Corrensstrasse 2,
  Münster 48149, Germany

transverse modes of a quasi-cw nanosecond control beam [16, 17]. In order to reduce pulse energy while keeping the pulse peak power fixed, it was recently proposed and numerically modeled to use femtosecond pulses for the probe and the control beam in a co-propagating setup [18]. This reduction in necessary pulse energy has been successfully realized experimentally achieving a reduction in about a factor of 150 in step-index fibers [19] as well as even a factor of 300 using a two-color approach in graded-index fibers [20]. A further decrease in pulse energy was predicted for using integrated optical waveguides and highly nonlinear materials [21].

Although first analytical expressions for OLPGs based on coupled mode equations have been derived already early in reference [16], so far predicting the efficiency of the all-optically induced gratings solely relies on numerical simulations either using a beam propagation method [22] for quasi-continuous-wave (quasi-cw) radiation or using the multi-mode generalized nonlinear Schrödinger equation (MM-NLSE) in the case of ultrashort pulses [18, 21, 23].

As a complement to these time-consuming numerical tools, an analytical framework for the description of cw- and ultrafast induced OLPGs will be presented here. Analytical expressions for the evolution of the modal contents of the probe beam were derived, which describe the energy evolution exactly in the cw-limit. Remaining limitations of the accuracy of the predicted mode conversion were found to arise for a mismatch in pulse duration or when the occurring group delay of the used ultrashort control and probe pulses is comparable to or even larger than their pulse duration. However, even in these unfavorable cases the analytical model allows to determine the order of magnitude of the achievable conversion at given fiber and control beam parameters. If more exact predictions are necessary, the results from the model can be used to quickly narrow the range of initial parameters for a full numerical simulation to save valuable numerical simulation time (minutes up to hours for a full simulation compared to milliseconds for evaluating the analytical expression). The analytical nature of the model, furthermore, accomplishes a direct insight into the physical process and allows to determine the major control pulse and waveguide parameters that govern the mode conversion.

2 Analytical model

OLPGs have been described theoretically via the induced change of the refractive index by the optical Kerr effect (material representation, [16]). The refractive index change being induced by the multi-mode interference of two control beam modes (amplitude A_j, $j = 1, 2$) and acting on two probe beam modes ($j = 3, 4$) can be evaluated by the

so-called coupled mode theory [24], very similar to the treatment of permanent long-period gratings. The resulting change in refractive index alongside the waveguide (z-direction),

$$n(x, y, z) = n_0'(x, y) + \Delta n(x, y) \cos(\Omega z - \phi_0), \quad (1)$$

with Δn being a function of the control beam power and $\Omega = \Delta\beta_c = \beta_1 - \beta_2$ of its propagation constants β_j directly leads to the coupled mode equations (see "Appendix 1" for details).

The solution in the material representation is equivalent to describing the interaction in a nonlinear wave interaction representation of four-wave mixing (see "Appendix 2"). The coupled mode equations can be directly derived from the four-wave mixing interaction between the modes p, l, m, n described in the MM-NLSE by the overlap integrals $Q_{plmn}^{(1,2)}$ (see reference [25] for details):

$$\begin{aligned}
\frac{\partial A_3}{\partial z} &= i\beta_3 \cdot A_3 + 4\frac{in_2\omega_0}{c}|A_1||A_2|\cos\left[(\beta_1 - \beta_2)z\right] \\
&\quad \cdot \left(Q_{3412}^{(1)}A_4 + Q_{3312}^{(1)}A_3\right) \\
&= i\beta_3 \cdot A_3 + iD_{34} \cdot A_4 + iD_{33}A_3,
\end{aligned} \quad (2)$$

with n_2 being the nonlinear index of refraction, ω_0 the angular frequency of the control beam and D_{34}, D_{33} the coupling coefficients. The equivalence of the two theoretical approaches connects the four-wave mixing interaction directly with transverse mode conversion for the first time and strengthens the physical interpretation of the mode conversion process in reference [18] being a result of optically induced long-period gratings.

After deriving the coupled mode equations for OLPGs, the results from standard coupled mode theory can be readily applied: The dimensionless phase mismatch σ normalized to the coupling strength between the induced grating and the two probe modes for OLPGs results in

$$\sigma = \frac{2}{\kappa}\{(\beta_1 - \beta_2) - (\beta_3 - \beta_4)\} = \frac{2}{\kappa}\Delta, \quad (3)$$

with $\kappa = \sqrt{\bar{D}_{34}\bar{D}_{43}} \propto |A_1||A_2|$ and $\Delta = \Delta\beta_c - \Delta\beta_p$ being the mismatch of the difference in propagation constants of the control and the probe modes. With an induced grating and assuming unit power in one probe mode ($j = 3$) and zero power in the other probe mode ($j = 4$) at the beginning of the fiber results in an asymptotic power transfer to the second probe mode of

$$P_4(z) = F^2 \sin^2\left(\frac{\kappa \cdot z}{2F}\right), \quad F = 1/\sqrt{\left(1 + \frac{\sigma^2}{4}\right)}. \quad (4)$$

The power in the first probe mode is always given by $P_3 = 1 - P_4$ due to energy conservation. The first deduction from Eqs. (3) and (4) is that the effective conversion

phase mismatch σ does not only depend on the difference in propagation constants of both modes (Δ), but is instead normalized to the coupling strength $\kappa \propto |A_1||A_2| = \sqrt{P_1 \cdot P_2}$ and thereby to the power of the control beam modes. The resulting power dependency of the conversion efficiency ($\eta = P_4/(P_3 + P_4)$) was also found in the numerical simulations presented in references [21, 23]. In these simulations, the decreasing effective conversion phase mismatch with control beam power was interpreted physically as an increasing conversion rate making up for the dephasing of the propagating probe and control modes.

Furthermore, when taking into account the first-order correction to the asymptotic solution from Eq. (4) in the phase-matched scenario ($\sigma = 0$, leading to $F = 1$), the power in mode $j = 4$ is given by [26]:

$$P_4(z) = \sin^2\left(\frac{\kappa \cdot z}{2}\right) - \frac{\kappa}{4\Delta\beta_p}\sin\left(2\Delta\beta_p \cdot z\right)\sin\left(\kappa \cdot z\right) \quad (5)$$

leading to a small oscillation of the modal power around the asymptotic solution with a period much shorter than the conversion length. The main contribution is still the asymptotic solution $\sin^2\left(\frac{\kappa \cdot z}{2}\right)$ that was already found in Eq. (4). The amplitude of the oscillations is given by the fraction $\kappa/\Delta\beta_p$, so that a very strong control beam as well as a very small difference in modal propagation constants in the probe beam would result in a large modulation of the energy transfer. A first investigation of this modulation was already done numerically for cw-control and probe beams [22], where it was observed, that the fast oscillations are connected to the mode beating period. This hypothesis has hereby been verified analytically, although the beating period of the probe modes is responsible for the modulation, and not that of the control beam modes as claimed in [22].

In order to verify the developed theoretical description of all-optical mode conversion, the calculated results can be compared to numerical simulations, e.g., using a scalar three-dimensional beam propagation method as demonstrated in reference [22]. The result of such a comparison is shown in Fig. 1: For the numerical simulation, two cross-polarized beams and a resulting nonlinear index of $n_2^{\text{XPM}} = \frac{2}{3} \cdot n_2$ has been chosen. The resulting evolution of the electrical field is shown decomposed into the modes of the waveguide, the black solid line showing the evolution of the LP$_{11}$-mode and the black dashed line the evolution of the fundamental mode. The modal powers derived from the OLPG coupled mode theory (OLPG-CMT) are displayed as the blue and red curve, respectively. Excellent agreement between the analytical model and the numerical simulation was found with a normalized rms deviation

$$\rho_{\text{rms}} = \frac{1}{N \cdot \bar{P}_4}\sum_{i=1}^{N}\left|P_{4,\text{sim}}(z_i) - P_{4,\text{CMT}}(z_i)\right|^2 \quad (6)$$
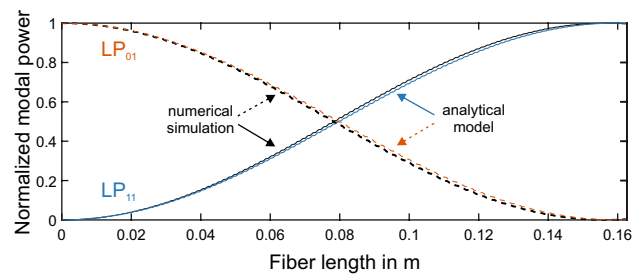
Fig. 1 Calculated all-optical cw power transfer from the LP$_{01}$ (*red dashed line*) to the LP$_{11}$ probe mode (*blue solid line*) in comparison with a numerical simulation relying on a three-dimensional beam propagation method (*dashed and solid black lines*). The control beam was assumed to be cross-polarized and at a power of 60 kW in each mode. Both beams were centered in wavelength around 1030 nm, and the fiber was a step-index fiber with a core diameter of 25 μm and a numerical aperture of about 0.06 at 1030 nm

of $\rho_{\text{rms}} = 0.03$, with $\bar{P}_4$ being the mean value of the modal power in the waveguide. Hence, the OLPG-CMT does represent a straightforward tool to estimate the power transfer for a given control beam power and phase mismatch.

3 Results and discussion

The developed analytical model can be applied to calculate the conversion efficiency η that one has to expect from an OLPG at a given control beam peak power and phase mismatch without the need for time-consuming numerical simulations. In order to provide a very general result that can be applied to virtually any waveguide, the conversion efficiency as well as the conversion length z_c, after which the conversion maximum is reached, is displayed in Fig. 2 a and b as a function of the coupling strength κ as well as the mismatch of the difference of the propagation constants Δ of the involved modes. The individual peak powers that will be necessary in a particular waveguide depend on the effective modal areas as well as the nonlinear coefficient of the used waveguide material [see Eqs. (20) and (31)]. For a graded-index fiber with a core diameter of 50 μm and a control beam center wavelength of 1030 nm, the corresponding peak powers in each control beam mode are displayed alongside κ as a reference. As was discussed in the last section, the conversion efficiency displayed in Fig. 2a drops when a phase mismatch Δ occurs between control and probe beam, and only by increasing the coupling strength a high efficiency can be regained reaching $\eta = 100\%$ in the limit of an infinite coupling strength. A different behavior is found for the conversion length shown in Fig. 2b which is reduced to shorter waveguide lengths with increasing phase mismatch as well as coupling strength. The displayed

(a)

Conversion efficiency η

(b)

Conversion length $\log_{10}(z_c)$ ($\log_{10}$(m))
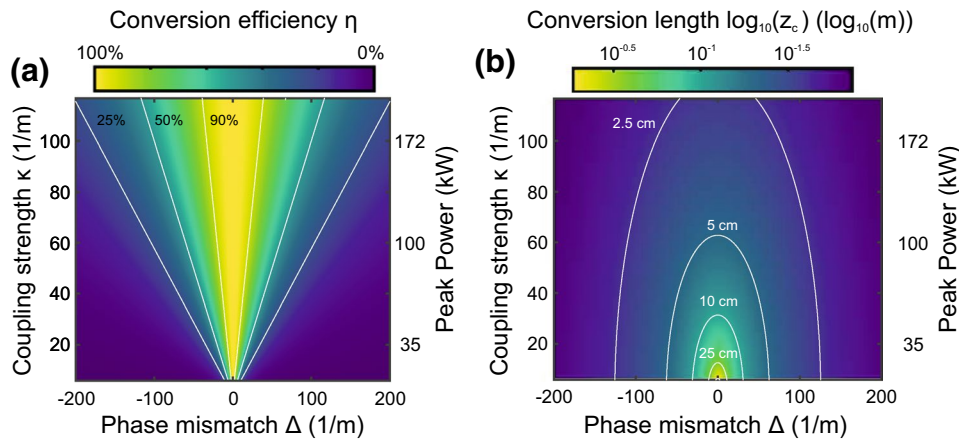
Fig. 2 Results of the analytical model of the all-optical cw power transfer between two higher-order modes as a function of the coupling strength κ as well as mismatch between the propagation constants of probe and control beam Δ. For reference, the corresponding peak power in a 50 μm graded-index fiber is given alongside κ for a control beam wavelength of 1030 nm. In **a** the conversion efficiency η is displayed color coded with contour *lines* indicating a set of fixed conversion efficiencies while in **b** the conversion length after which maximum conversion is achieved is shown on a logarithmic scale

false color plots allow to quickly estimate the expected efficiency of a conversion process and the needed length of the waveguide for planning an experiment.

However, note that the presented results are only exact in the cw-limit. In order to explore the usefulness of the presented results for pulsed applications, we conducted a systematic study by comparing the results of the theoretical model with full simulations of the MM-NLSE in a graded-index fiber and by taking into account the nonlinear interactions between the pulses as well as dispersive broadening and walk-off ($\Delta = 7.3$/m, $\kappa = 20.3$/m—corresponding to a peak power of 40 kW in each control mode at a center wavelength of 1030 nm and a probe beam wavelength of 1300 nm). In general, a deviation of the results can be expected from two main contributions: (1) If probe and control pulses are of similar duration or the control pulses are even shorter than the probe pulses, the grating (coupling) strength κ will vary at different temporal positions of the probe pulse. When the cw-model would predict a complete conversion at a certain peak power of the control pulse, e.g., some remaining energy in the pulse wings was observed in numerical simulations [18]. (2) Even for probe pulses considerably shorter than the control pulses, meaning the coupling strength is nearly uniform, the cw-model can fail if strong pulse walk-off occurs. In this case, the coupling strength, while being uniform for the probe pulse at each waveguide position, will decrease along the waveguide.

In order to study both of these cases, we varied the ratio t_c/t_p of the control and probe pulse duration from equal durations up to five times longer control than probe pulses. Furthermore, for a fixed ratio of pulse durations we varied the occurring group delay relative to the control pulse duration ranging from 10 % up to over 100 %. This was achieved by scaling the control pulse durations (t_c from 500 fs to 5 ps) while keeping the fiber length and parameters and thereby the occurring absolute group delay ($\Delta\tau$ about 521 fs) fixed. For each combination of pulse duration ratios and relative group delay, we then calculated the normalized rms deviation ρ_{rms} of the power in the higher-order mode in comparison with the powers calculated with the cw-model assuming cw-control powers equal to the peak power of the control pulses. The resulting rms deviations are displayed in Fig. 3a. As it was expected, the error of the cw-model dropped with increasing pulse duration ratio between the control and the probe pulses and saturated toward a ratio of five. Furthermore, the influence of the group delay became significant when surpassing half the control pulse duration. The mean squared error for short probe pulses at relative group delays bigger than 70–80 % was found to be equivalent to the error of equal probe to control pulse durations at low group delay.

In Fig. 3b, c, the predicted power in the higher-order mode is plotted for the cw-model and compared to the result of a numerical simulation during one conversion cycle for parameters indicated by gray circles in Fig. 3a to give an impression of the occurring deviation between both models. In Fig. 3b, the control pulses are assumed to be of the same duration as the probe pulses resulting in a relatively large rms error of more than $\rho_{rms} = 0.4$. The large rms error resulted from the cw-model (depicted by the dashed black line) clearly overestimating the occurring mode conversion in comparison with the full numerical simulation (red solid line) for the reasons given above. In contrast, the conversion along the fiber for five times shorter probe than control pulses is displayed in Fig. 3c and
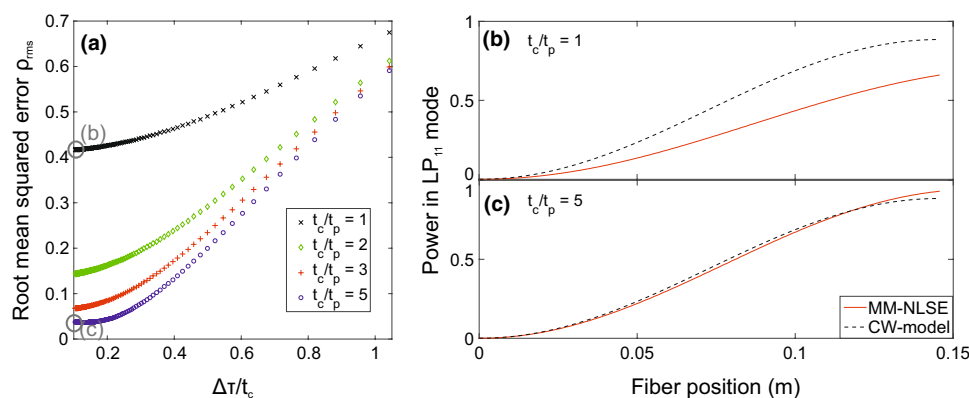
Fig. 3 **a** The normalized root-mean-square error ρ_{rms} of the cw-model in comparison with full numerical simulations using the MM-NLSE as a function of occurring group delay $\Delta\tau$ relative to the control pulse duration t_c. Furthermore, in **b** and **c** a detailed analysis of the power transfer into the higher-order mode along the waveguide is shown for different pulse duration ratios t_c/t_p between control and probe pulse (marked with *gray circles* in **a**))

shows very good agreement corresponding to an rms error of less than $\rho_{rms} = 0.04$.

The points discussed above show the benefits as well as limitations of the developed model and allow to classify the results given by the model: For control pulses significantly longer than the probe pulse in combination with a negligible group delay within one conversion length, the results of the analytical model can directly be used as a very good approximation for the expected conversion efficiency. When these requirements are not met, the results from the analytical model can still be used to get an understanding of the expected order of magnitude of the conversion efficiency in dependence of the fiber length and control pulse power. As the analytical model allows to calculate results within milliseconds, these results can be used as appropriate predictions to drastically lower the amount of initially free parameters for a more exact numerical simulation or even for an experimental verification.

4 Conclusion

In this manuscript, an analytical description of optically induced long-period gratings was presented connecting for the first time the material representation with an ultrashort pulse induced four-wave mixing interaction. It was successfully demonstrated that the all-optical mode conversion process can be described either in a material representation, in which the local modes are altered and the resulting energy transfer is described by coupled mode equations, or alternatively in a four-wave mixing representation, derived from the coupled nonlinear Schrödinger equations. Both approaches led to the same analytical description of the energy transfer that is supposed to exactly describe the process in the long-pulse or quasi-continuous-wave regime.

The developed model was compared to numerical simulations that have already been published elsewhere, describing the conversion process in the material representation [22] as well as in the four-wave mixing representation [18]. Excellent agreement was found for comparison to continuous-wave simulations, while modeling nonlinear transverse mode conversion with ultrashort pulses was shown to depend on occurring pulse walk-off, leading to a deviation from the analytical model when the walk-off is becoming significant. Despite these shortcomings, the presented analytical model allowed to gain insight into the physical dependence of the conversion efficiency on the control beam power and the normalized phase mismatch. Due to the analytical nature of the description of the conversion process, the developed model allows to directly estimate (within milliseconds) the maximum achievable mode conversion for any combination of control beam and waveguide parameters (e.g., control power and center wavelengths, initial phases) without having to rely on numerical simulations (calculation time of hours for a single initial parameter set) and, hence, saving valuable computation time.

Appendix 1: Material representation

In this section, coupling coefficients of an optically induced long-period grating are derived in detail in the material representation, i.e., describing the mode conversion process with coupled mode theory. The coupling of transverse modes by a sinusoidal perturbation of the refractive index, as it is the case by a periodic long-period grating, has been described already by Snyder in 1972 [24] before first experimental results have been discussed. The resulting so-called coupled mode theory is very well described

in several textbooks [26, 27] as well as papers [28] and in this section only the necessary modifications to describe all-optically induced long-period gratings are given. The nomenclature and mode normalization is the same as in Snyder [26] so that the analytical signal of the electrical field $\mathbf{E}(x, y, z)$ of the forward-propagating bound modes of a translation invariant optical waveguide is given by:

$$\mathbf{E}(x, y, z) = \sum_j A_j \mathbf{E}_j(x, y, z), \tag{7}$$

$$\mathbf{E}_j(x, y, z) = \hat{\mathbf{e}}_j(x, y) \exp(i\beta_j z). \tag{8}$$

Here, the frequency-dependent propagation constant or eigenvalue of the jth mode is called $\beta_j(\omega)$, whereas the kth coefficient of its Taylor series centered at ω_0 will be given as $\beta_j^{(k)}$. The transverse electric field distributions $\hat{\mathbf{e}}_j(x, y)$ and magnetic field distributions $\hat{\mathbf{h}}_j(x, y)$ contain the implicit time dependence $\exp(-i\omega_0 t)$ and are considered orthonormal with regards to the definition given in reference [26]:

$$\frac{1}{2} \int_{A_\infty} \hat{\mathbf{e}}_j \times \hat{\mathbf{h}}_k^* \cdot \hat{\mathbf{z}} dA = \begin{cases} 1, & \text{if } j = k \\ 0, & \text{if } j \neq k. \end{cases} \tag{9}$$

The total power P_j of one mode propagating in the z-direction is, therefore, given by the modal expansion coefficient A_j:

$$P_j = |A_j|^2. \tag{10}$$

The electrical field of the multi-mode interference of two control modes can be described as:

$$\begin{aligned} \mathbf{E}(x, y, z) = \, & A_1 \hat{\mathbf{e}}_1(x, y) \exp(i\beta_1 z) \\ & + A_2 \hat{\mathbf{e}}_2(x, y) \exp(i(\beta_2 z + \phi_0)), \end{aligned} \tag{11}$$

with $A_1, A_2 \in \mathbb{R}$ and with a relative phase of ϕ_0 between the two modes. The Kerr-induced local refractive index experienced by the probe beam is proportional to the control beam intensity $I(x, y, z)$ and given by

$$n(x, y, z) = n_0 + n_2^{\text{XPM}} \cdot I(x, y, z). \tag{12}$$

As the index change is induced by cross-phase modulation (XPM), the nonlinear index n_2^{XPM} differs from the regular nonlinear index n_2 known from, e.g., self-phase modulation by a factor of $n_2^{\text{XPM}} = 2n_2$ for two beams with the same polarization and $n_2^{\text{XPM}} = \frac{2}{3}n_2$ for two cross-polarized beams in cylindrically symmetric optical fibers [29]. The induced index change is proportional to the multi-mode interference intensity or power density pattern that can be calculated from the z-component of the Poynting vector $I = \langle S_z \rangle$ [26]. If the longitudinal component of the electrical field e_z can be neglected in comparison with its transverse components, as it is the case in the weakly guiding regime, the mode fields $\hat{\mathbf{e}}_j$ under investigation in this section can be transformed to be completely real valued. When, furthermore, assuming $\beta_1 \approx \beta_2 \approx \frac{2\pi n_0}{\lambda_0}$ for calculating the

magnitude of the modal intensities (both are of the order of magnitude $10^6/m$), the power density reduces to

$$\begin{aligned} \langle S_z \rangle &= \left\langle \frac{1}{2} \text{Re} \left(\mathbf{E} \times \mathbf{H}^* \right) \hat{\mathbf{z}} \right\rangle \\ &= \frac{n_0}{2} \sqrt{\frac{\epsilon_0}{\mu_0}} \left\{ |A_1|^2 |\hat{\mathbf{e}}_1(x, y)|^2 + |A_2|^2 |\hat{\mathbf{e}}_2(x, y)|^2 \right. \\ &\left. + 2A_1 A_2 \hat{\mathbf{e}}_1(x, y) \cdot \hat{\mathbf{e}}_2(x, y) \cos(\Omega z - \phi_0) \right\}, \end{aligned} \tag{13}$$

with n_0 being the refractive index of the core of the fiber, λ_0 the wavelength of the light in vacuum and the angular wave number $\Omega = \beta_1 - \beta_2$, here, the approximation used for the magnitude of the modulation is not valid as for the phase of the cosine the small difference between β_1 and β_2 is of significance. The resulting changed refractive index,

$$n(x, y, z) = n_0'(x, y) + \Delta n(x, y) \cos(\Omega z - \phi_0), \tag{14}$$

can be interpreted as a z-independent change of the nominal refractive index $n_0(x, y)$ due to an added constant offset

$$\begin{aligned} n_0'(x, y) &= n_0(x, y) + \frac{1}{2}n_2^{\text{XPM}} \cdot n_0 \sqrt{\frac{\epsilon_0}{\mu_0}} \\ &\quad \cdot \left\{ |A_1|^2 |\hat{\mathbf{e}}_1(x, y)|^2 + |A_2|^2 |\hat{\mathbf{e}}_2(x, y)|^2 \right\} \end{aligned} \tag{15}$$

and an interference term that leads to a cosinusoidal modulation of the refractive index with magnitude

$$\Delta n(x, y) = n_2^{\text{XPM}} \cdot n_0 \sqrt{\frac{\epsilon_0}{\mu_0}} A_1 A_2 \hat{\mathbf{e}}_1(x, y) \cdot \hat{\mathbf{e}}_2(x, y). \tag{16}$$

For the coupling of transverse modes, the square of the refractive index (or the permittivity) is the relevant material parameter, which can be calculated to

$$\begin{aligned} n^2(x, y, z) &= n_0'^2(x, y) + 2n_0' \cdot \Delta n(x, y) \cos(\Omega z - \phi_0) \\ &\quad + \mathcal{O}(\Delta n^2) \approx n_0'^2(x, y) + 2n_0' \Delta n \cos(\Omega z - \phi_0). \end{aligned} \tag{17}$$

The coupling coefficients for an optically induced long-period grating can, therefore, be reduced to the same form as in the standard coupled mode equations in reference [26] with $\delta n^2 = 2n_0'(x, y) \cdot \Delta n(x, y)$, when the initial phase between both control beam modes is $\phi_0 = \pi/2$. In order to directly adapt the results from [26], the relative phase between the two control modes is assumed to be $\phi_0 = \pi/2$ for the rest of this section. As the all-optically induced refractive index change can then be reduced to the same type of equation as for a conventional sinusoidally shaped long-period grating, the asymptotic solution, describing the energy transfer from one mode to another, as well as the higher-order corrections leading to a modulation of the energy transfer, can be readily taken from reference [26] to describe the cw-limit of all-optical mode conversion. The coupled mode equations in this case are

$$\frac{\partial A_3}{\partial z} = i\beta_3 \cdot A_3 + iD_{34} \cdot A_4 + iD_{33}A_3, \tag{18}$$

$$\frac{\partial A_4}{\partial z} = i\beta_4 \cdot A_4 + iD_{43} \cdot A_3 + iD_{44}A_4. \tag{19}$$

The coupling coefficient for two probe modes ($j = 3, 4$) determined by the index grating induced by control modes ($j = 1, 2$), which is the main result of this section, is then given by

$$D_{34} = \bar{D}_{34} \cdot \sin(\Omega z)$$
$$\bar{D}_{34} = n_2^{\text{XPM}} \cdot \frac{k}{2} n_0^2 \frac{\epsilon_0}{\mu_0} A_1 A_2 \int_{A_\infty} (\hat{\mathbf{e}}_1 \cdot \hat{\mathbf{e}}_2)(\hat{\mathbf{e}}_3 \cdot \hat{\mathbf{e}}_4)\, \mathrm{d}A, \tag{20}$$

with the integral of the area element dA over the total mode area.

Appendix 2: Four-wave mixing representation

The theoretical description of OLPGs given in the last section can be interpreted as a periodic perturbation of the local probe modes of the waveguide by the refractive index change induced by the control beam. This description is well suited for long pulses in the picosecond regime or ultimately in the cw-limit. In this section, the all-optical mode conversion will be described in detail in the four-wave mixing representation derived from the multi-mode generalized nonlinear Schrödinger equations (MM-NLSE) presented by Poletti and Horak [25]. This set of equations can be used to accurately describe the nonlinear interaction of different transverse modes even for ultrashort pulses. It will be shown that the description of an optically induced grating by the MM-NLSE is equivalent to the material representation of Sect. 1 in the cw-limit and is, therefore, perfectly suited for numerically modeling the conversion process in case ultrashort pulses are used.

The evolution of the complex modal amplitude $A_p(t, z)$ as formulated in reference [25] is given by the following coupled equations:

$$\begin{aligned}\frac{\partial A_p}{\partial z} =& i\left(\beta_p^{(0)} - \beta^{(0)}\right)A_p + D_p(A_p) \\ &+ \frac{in_2\omega_0}{c} \sum_{l,m,n} \left\{ \left(1 + i\tau_{plmn}^{(1)} \frac{\partial}{\partial t}\right) \cdot 2Q_{plmn}^{(1)}A_l \right. \\ &\cdot \int R(\tau)A_m(t-\tau)A_n^*(t-\tau)\mathrm{d}\tau + \left(1 + i\tau_{plmn}^{(2)} \frac{\partial}{\partial t}\right) \\ &\left. \cdot Q_{plmn}^{(2)}A_l^* \cdot \int R(\tau)A_m(t-\tau)A_n(t-\tau)e^{2i\omega_0\tau}\mathrm{d}\tau \right\}, \end{aligned} \tag{21}$$

with $\beta_p^{(j)}$ being the jth Taylor series coefficient of the propagation constant β of the pth mode, D_p the dispersion operator, $Q_{plmn}^{(1,2)}$ the coupling coefficients between the transverse modes, τ_{plmn} the shock-time coefficients and $R(\tau)$ the delayed Raman response of the waveguide. In order to derive the mode conversion efficiency in the long-pulse or quasi-cw approximation, dispersion as well as self-steepening or the Raman effect can be neglected reducing the coupled equations to the simpler form

$$\begin{aligned}\frac{\partial A_p}{\partial z} =& i\left(\beta_p^{(0)} - \beta^{(0)}\right)A_p + \frac{in_2\omega_0}{c} \\ &\cdot \sum_{l,m,n} \left\{ 2Q_{plmn}^{(1)}A_lA_mA_n^* + Q_{plmn}^{(2)}A_l^*A_mA_n \right\}. \end{aligned} \tag{22}$$

At first, the case of a strong control beam being distributed between two modes ($p = 1, 2$) and also being cross-polarized to the probe beam is considered. With the power of the control beam being much higher than that of the two probe modes ($p = 3, 4$, $P_1 \approx P_2 \gg P_3 \approx P_4$), changes of the control beam induced by the probe beam can be easily disregarded. This treatment can be compared to the case of an undepleted pump beam in conventional four-wave mixing and leads to an unperturbed control beam and to a straightforward description of the modal coefficients of the control beam

$$A_p(z, t) = |A_p(t)| \cdot \exp\left(i\beta_p^{(0)} \cdot z\right), \tag{23}$$

with $p = 1, 2$. In contrast to four-wave mixing amplification, the self- and cross-phase modulation of the control beam itself can be neglected in a first approximation as well as only phase differences between the modes are of interest, and the difference in acquired nonlinear phase between the two control modes is usually small. The small probe beam power (usually two to three orders of magnitude smaller than the control beam), furthermore, allows to disregard all terms in the sum over l, m and n in Eq. (22) which contain any product of A_3 and A_4, as it will be small in comparison with a product containing at least two of the control beam modal coefficients (A_1 and/or A_2). Finally, noting that in case of a cross-polarized control and probe beam $Q_{3lmn} = 0$ for $l \neq 3, 4$ [25], we end up with the following equation for the change in amplitude of the probe mode 3 ($A_3(z, t)$, omitting the superscript index at $\beta_j^{(0)}$ for better readability):

$$\begin{aligned}\frac{\partial A_3}{\partial z} =& i\beta_1 A_3 + \frac{in_2\omega_0}{c}\left\{ A_4 \left(2Q_{3412}^{(1)} \cdot |A_1||A_2| \cdot e^{i(\beta_1 - \beta_2)z} \right. \right. \\ &\left. \left. + 2Q_{3421}^{(1)} \cdot |A_2||A_1| \cdot e^{i(\beta_2 - \beta_1)z} \right) \right. \end{aligned} \tag{24a}$$

$$+ A_3 \left(2Q_{3312}^{(1)} \cdot |A_1||A_2| \cdot e^{i(\beta_1 - \beta_2)z} \right.$$
$$\left. + 2Q_{3321}^{(1)} \cdot |A_2||A_1| \cdot e^{i(\beta_2 - \beta_1)z} \right) \tag{24b}$$

$$+ A_3 \left(2Q_{3311}^{(1)} \cdot |A_1|^2 + 2Q_{3322}^{(1)} \cdot |A_2|^2 \right) \tag{24c}$$

$$+ A_4 \left(2Q_{3411}^{(1)} \cdot |A_1|^2 + 2Q_{3422}^{(1)} \cdot |A_2|^2 \right)$$
$$+ A_3^* \left(Q_{3311}^{(2)} \cdot |A_1|^2 \cdot e^{i2\beta_1 z} + Q_{3322}^{(2)} \cdot |A_2|^2 \cdot e^{i2\beta_2 z} \right.$$
$$\left. + Q_{3312}^{(2)} \cdot |A_1||A_2| \cdot e^{i(\beta_1 + \beta_2)z} + Q_{3321}^{(2)} \cdot |A_2||A_1| \cdot e^{i(\beta_2 + \beta_1)z} \right)$$
$$+ A_4^* \left(Q_{3411}^{(2)} \cdot |A_1|^2 \cdot e^{i2\beta_1 z} + Q_{3422}^{(2)} \cdot |A_2|^2 \cdot e^{i2\beta_2 z} \right.$$
$$\left. + Q_{3412}^{(2)} \cdot |A_1||A_2| \cdot e^{i(\beta_1 + \beta_2)z} + Q_{3421}^{(2)} \cdot A_4^* |A_2||A_1| \cdot e^{i(\beta_2 + \beta_1)z} \right) \bigg\}.$$
$$\tag{24d}$$

The according equation for A_4 can be obtained by exchanging the index 3 with the index 4 and vice versa for the terms A, β and Q. The two terms in Eq. (24c), containing the coupling coefficients $Q_{3311}^{(1)}$ and $Q_{3322}^{(1)}$, constitute the XPM acting from the control beam on the probe beam that can be identified with the constant refractive index offset introduced in Eq. (15). In the considered scenario, XPM as well as SPM can be approximated as being of the same strength for both control beam modes, except for a slight dependence on the difference in transverse mode shape. As for phase matching only relative phase differences matter, we neglect these terms in the following as a constant phase contribution during propagation. The term labeled (24d) and the following terms are considered non-phase-matched terms. Assuming a nearly phase-matched mode conversion scenario with $\beta_1 - \beta_2 \approx \beta_3 - \beta_4$, in general, these terms oscillate with a frequency relative to A_3 that is very fast in comparison with the phase-matched contributions from Eq. (24a). Therefore, the terms following Eq. (24d) do not contribute to the energy exchange, resulting in a description of the energy transfer as an asymptotic solution governed by the $Q^{(1)}$ coupling coefficients of Eq. (24a). While this assumption cannot exactly be justified easily a priori, it will be shown that it leads to the correct description of the all-optically induced mode conversion. The remaining terms denote a coupling of the amplitude of probe mode 3 (A_3) to probe mode 4 (A_4) described by the terms in (24a) as well as a self-coupling (24b), both induced by the magnitude of the two control modes ($|A_1|$ and $|A_2|$). With these assumptions and recognizing that

$$Q_{34} := Q_{3412}^{(1)} = Q_{3421}^{(1)} = Q_{43} := Q_{4312}^{(1)} = Q_{4321}^{(1)} \tag{25}$$

$$Q_{33} := Q_{3312}^{(1)} = Q_{3321}^{(1)}, \tag{26}$$

we end up with the following two coupled equations for the modal coefficients of both probe modes A_3 and A_4:

$$\begin{aligned}
\frac{\partial A_3}{\partial z} &= i\beta_3 \cdot A_3 \\
&\quad + 4\frac{in_2\omega_0}{c}|A_1||A_2| \\
&\quad \times \cos\left[(\beta_1 - \beta_2)z\right] \cdot (Q_{34}A_4 + Q_{33}A_3) \\
&= i\beta_3 \cdot A_3 + iD_{34}' \cdot A_4 + iD_{33}'A_3
\end{aligned} \tag{27}$$

$$\frac{\partial A_4}{\partial z} = i\beta_4 \cdot A_4 + iD_{43}' \cdot A_3 + iD_{44}'A_4 \tag{28}$$

These two equations are of identical form to the coupled mode equations derived in reference [26]. Using the definition for the Q's of reference [25], the coupling coefficients can be expressed as:

$$\begin{aligned}
D_{34}' &= 4\frac{n_2\omega_0}{c}|A_1||A_2|\cos(\beta_1 - \beta_2)z \\
&\quad \cdot \frac{n_0^2\epsilon_0}{12\mu_0}\int_{A_\infty} \left(\hat{\mathbf{e}}_3\hat{\mathbf{e}}_4\right) \cdot \left(\hat{\mathbf{e}}_1\hat{\mathbf{e}}_2\right) \mathrm{d}A
\end{aligned} \tag{29}$$

$$= \bar{D}_{34}' \cdot \sin(\beta_1 - \beta_2), \tag{30}$$

with

$$\begin{aligned}
\bar{D}_{34}' &= \frac{2n_2}{3}\frac{k}{2}n_0^2\frac{\epsilon_0}{\mu_0} \\
&\quad \cdot |A_1||A_2|\int_{A_\infty} \left(\hat{\mathbf{e}}_3\hat{\mathbf{e}}_4\right) \cdot \left(\hat{\mathbf{e}}_1\hat{\mathbf{e}}_2\right) \mathrm{d}A.
\end{aligned} \tag{31}$$

Comparing the coefficients D_{34}' and D_{43}' with the coupling coefficients D_{34} and D_{43} introduced in Eq. (20), furthermore, reveals that they are indeed identical to the cross-polarized case in the material representation. Extending the analysis described above for the co-polarized case is easily done by acknowledging that $Q_{3lmn} \neq 0$ also for $l \neq 3, 4$ is leading to additional nonzero contributions that change the value of the fractional in front of the nonlinear index in Eq. (31) to $2 \cdot n_2$. Thereby, it is shown that describing the OLPG by the four-wave mixing interaction that can be numerically modeled by solving the multi-mode coupled nonlinear Schrödinger equations is equivalent to the solution of the coupled mode perturbation theory in the long-pulse or quasi-cw regime. This equivalence analytically verifies that indeed the numerically observed transverse mode conversion during nonlinear interaction of probe and control beams physically originates from an optically induced long-period grating.

References

1. K. Hill, B. Malo, K. Vineberg, F. Bilodeau, D. Johnson, I. Skinner, Electron. Lett. **26**, 1270–1272 (1990)
2. A.A.M. Vengsarkar, P.J.P. Lemaire, J.B.J. Judkins, V. Bhatia, T. Erdogan, J.E.J. Sipe, J. Light. Technol. **14**, 58–65 (1996)
3. T. Erdogan, J. Opt. Soc. Am. A **17**, 2113 (2000)
4. Y.-J. Rao, Y.-P. Wang, Z.-L. Ran, T. Zhu, J. Light. Technol. **21**, 1320–1327 (2003)
5. A.M. Vengsarkar, J.R. Pedrazzani, J.B. Judkins, P.J. Lemaire, N.S. Bergano, C.R. Davidson, Opt. Lett. **21**, 336–338 (1996)
6. C. Poole, J. Wiesenfeld, D. DiGiovanni, A. Vengsarkar, J. Light. Technol. **12**, 1746–1758 (1994)
7. S. Ramachandran, J. Light. Technol. **23**, 3426–3443 (2005)
8. J.W. Nicholson, S. Ramachandran, S. Ghalmi, Opt. Express **15**, 6623–6628 (2007)
9. B.Y. Kim, J.N. Blake, H.E. Engan, H.J. Shaw, Opt. Lett. **11**, 389–391 (1986)
10. H.E. Engan, B.Y. Kim, J.N. Blake, H.J. Shaw, J. Light. Technol. **6**, 428–436 (1988)
11. J. Zhao, X. Liu, Opt. Lett. **31**, 1609–1611 (2006)
12. D.J. Richardson, J.M. Fini, L.E. Nelson, Nat. Photonics **7**, 354–362 (2013)
13. J. Carpenter, B.C. Thomsen, T.D. Wilkinson, J. Light. Technol. **30**, 3946–3952 (2012)
14. N. Amaya, M. Irfan, G. Zervas, R. Nejabati, D. Simeonidou, J. Sakaguchi, B.J. Puttnam, T. Miyazawa, Y. Awaji, N. Wada, I. Henning, Opt. Express **21**, 8865–8872 (2013)
15. D.-R. Song, H.S. Park, B.Y. Kim, K.Y. Song, J. Light. Technol. **32**, 4534–4538 (2014)
16. H.G. Park, S.Y. Huang, B.Y. Kim, Opt. Lett. **14**, 877–878 (1989)
17. N. Andermahr, C. Fallnich, Opt. Express **18**, 4411–4416 (2010)
18. T. Walbaum, C. Fallnich, Appl. Phys. B **115**, 225–235 (2013)
19. T. Hellwig, M. Schnack, T. Walbaum, S. Dobner, C. Fallnich, Opt. Express **22**, 24951–24958 (2014)
20. M. Schnack, T. Hellwig, M. Brinkmann, C. Fallnich, Opt. Lett. **40**, 4675 (2015)
21. T. Hellwig, J.P. Epping, M. Schnack, K.-J. Boller, C. Fallnich, Opt. Express **23**, 19189–19201 (2015)
22. M. Schäferling, N. Andermahr, C. Fallnich, Appl. Phys. B **102**, 809–817 (2011)
23. T. Hellwig, T. Walbaum, C. Fallnich, Appl. Phys. B **112**, 499–505 (2013)
24. A.W. Snyder, J. Opt. Soc. Am. **62**, 1267–1277 (1972)
25. F. Poletti, P. Horak, J. Opt. Soc. Am. B **25**, 1645–1654 (2008)
26. A.W. Snyder, J.D. Love, *Optical Waveguide Theory* (Kluwer Academic Publishers, London, 1983)
27. J. Bures, *Guided Optics* (Wiley, New York, 2009)
28. T. Erdogan, J. Light. Technol. **15**, 1277–1294 (1997)
29. R.W. Boyd, *Nonlinear Optics* (Academic Press, Boston, 2008)